Experimental Investigation on the Pore-Scale Mechanism of Improved Sweep Efficiency by Low-Salinity Water Flooding Using a Reservoir-on-a-Chip

Songqi Li, Yuetian Liu,* Liang Xue,* Li Yang, and Zhiwang Yuan

Read Online

ACCESS | Metrics & More | Article Recommendations

High salinity water flooding → Low salinity water flooding
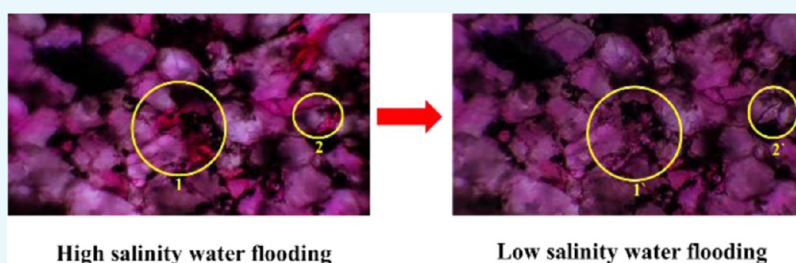
ABSTRACT: Low-salinity water flooding, known as an environmentally friendly and efficient oil recovery technology, has attracted the attention of several researchers all over the world. However, its field application is suffering restrictions because of the ambiguous mechanisms of the oil recovery by controlling the salinity. In this study, a water flooding microfluidic experiment was conducted to investigate the pore-scale mechanism of enhanced sweep efficiency by low-salinity water flooding. This experiment used a reservoir-on-a-chip that preserved the real rock properties and morphological features. Crude oil−water−rock contact angle experiments by altering water salinity were conducted to investigate the mechanism of the improvement of sweep efficiency by low-salinity water flooding. The experiment results show that unlike high-salinity water flooding, low-salinity water flooding improves its sweep efficiency from wettability alteration. Specifically, in the microfluidic model, it clearly shows that the pore-scale sweep efficiency is improved by reducing the salinity of injected water. Low-salinity water can invade the pores that cannot be reached by high-salinity water and displace the remaining oil after high-salinity water flooding. In the altering water salinity contact angle experiments, the contact angles decrease from 91.05° (neutral-wet) to 64.41° (water-wet) as the water salinity decreases from 46.58 to 2.31 g/L. The wettability of the rock surface changes from oil or neutral-wet to water-wet and induces the imbibition process, during which the hydrophilic pores absorb the low-salinity water into the smaller pores where the high-salinity water cannot invade. This investigation provides a further in situ and pore-scale evidence of improved sweep efficiency and wettability alteration by low-salinity water flooding and a possible reference to solve the difficulty in upscaling fluid flow behavior from microfluidics to reservoir rocks.

1. INTRODUCTION

Water flooding is known as the most widely used oil recovery technology in oil recovery all over the world.[1,2] However, a series of problems, including fast water cut rising and low water flooding recovery, have arisen as the development continues that seriously restrict oil production in many oil fields.[3] Petroleum engineers and researchers are trying to find ways to prevent the problems and enhance the oil recovery, such as nanotechnology,[4] DC voltage,[5,6] thermal recovery,[7] non-Darcy flow performance, and computational fluid dynamics (CFD) technology.[8,9] While these concerns should give a renewed boost to new recovery technologies, their potential is still small relative to the world's future needs.

Low-salinity water flooding (LSWF) is considered as a potential enhanced oil recovery (EOR) method due to its high efficiency and environment friendliness, and a number of studies on this topic have been published in recent years as a result of the growing interest in academia and industry.[10−12] In practice, however, the underlying mechanism and pore-scale flow dynamics in a real reservoir are still not well understood as the water flooding performance and oil configuration in the porous rock still remain unaddressed.[13,14] The unknown mechanisms limit the field application of low-salinity water (LSW) flooding, and this motivated us to investigate the pore-scale flooding performance and mechanisms.
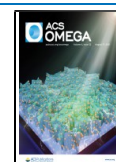
One of the most attractive research areas about low-salinity water flooding is the wettability alteration from oil-wet or neutral-wet to water-wet by reducing the salinity of injected water. It is believed to be the directly controlling cause of the EOR by low-salinity water flooding although more than one mechanism might contribute to the improved recovery.[15,16] Pore-scale visual water flooding microfluidic experiment has been receiving significant interest, and many papers have been published to report the newest research results using a micromodel. Mohammadi and Mahani fabricated a calcite micromodel to investigate the pore-scale mechanism of low-salinity water flooding in carbonates, and their results showed that the recovery efficiency was improved and wettability was changed to a more water-wet state as the brine salinity lowered.[17] Du presented a study of the low-salinity effect during oil recovery using a microfluidic experiment, and their experiment at the pore scale revealed a time-dependent oil dewetting and swelling behavior.[18] Mahzari and Sohrabi conducted a micromodel experiment and Fourier transform infrared (FTIR) tests, and they reported that the propensity of oil to form microdispersions played crucial roles in the efficiency of low-salinity water injection.[19] Aldousary and Kovscek investigated the process of spontaneous emulsification from a pore-scale perspective using a microfluidic experiment, and they concluded that diffusion of water into the crude oil phase was important for the formation of water-in-oil emulsions. Polar components in the oil phase might be important for stabilizing these emulsions.[20] Barnaji and Pourafshary made a visual clay-coated porous medium to study the effects of clay minerals on the enhancement of oil recovery by low-salinity water flooding. LSWF would be more effective in the clay-coated porous media with high cation-exchange-capacity clay in the primary mode, and it increased the interstitial velocity in some pore paths due to pore-plugging by swelling of clay and finally led to sectional sweeping.[21] Alfi and Nasrabadi used the lab-on-a-chip technology to investigate the confinement effect on the phase behavior of hexane, heptane, and octane.[22]

Oil−water−rock interaction at pore scale is very important for oil recovery. Incremental oil recovery has been observed from both clay and non-clay-bearing sandstones where different mechanisms have been put forward by different researchers and research groups even at the molecular level. Mehraban carried out a series of microfluidic water flooding experiments without clay. They observed that the micro-dispersion caused by the acidic compounds within the crude oil plays a leading role in oil swelling and wettability alteration in a porous medium that leads to an increase in the microscopic sweeping efficiency, thus leading to improved oil recovery.[23] The work showed the release of adsorbed oil not only from the surface of the minerals (pore lining materials) due to wettability change but also from the interlayer surfaces of the clay minerals or spontaneous formation of water microdispersion. Reducing the salinity increases the interfacial tension.[24] Sanyal reported the effect of clay mineral on oil recovery during low-salinity water flooding. Both the cations in the brine and kaolinite composition can influence the oil recovery.[25] Furthermore, the type of cations present on the surface of montmorillonite and the size of polycyclic aromatic hydrocarbon in asphaltenes affect the interaction phenomenon. This provides molecular-level insights into montmorillonite and brine, which are necessary to design optimal injection fluids for the EOR.[26−28]

However, in practice, many researchers select glass or calcite as a material to fabricate the micromodel as an approximate method to build a pore-scale model for the reasons of performance, cost, technology limitations, and so on. This approach however is limited by the lack of natural surface and mineral heterogeneity that dictates pore-scale flow dynamics and can be effective only when the solid−liquid interaction, such as wettability, can be ignored. However, as the water flooding continues, it is necessary for petroleum scientists to focus on the displacement of boundary layer fluid in a porous reservoir. Naturally occurring petroleum reservoirs contain significant varieties of minerals showing different wettabilities, such as the water-wet quartz and oil-wet clay in sandstone reservoir and dolomite and limestone in carbonate reservoir.[29] The glass or calcite micromodel can only imitate the pore structure instead of mineral components of the reservoir rock.

In this work, a real reservoir-on-a-chip was fabricated to guarantee the similarity between an experimental model and a real reservoir. A water flooding microfluidic experiment was conducted to investigate the pore-scale mechanism of enhanced sweep efficiency, and contact angle measurements were carried out at different levels of water salinity to investigate the influence of water salinity on wettability alteration. The result of microfluidic experiment showed that low-salinity water invaded the pores that cannot be reached by high-salinity water (HSW) and displaced the remaining oil after high-salinity water flooding. In the altering water salinity contact angle experiments, the contact angles decreased from 91.05° (neutral-wet) to 64.41° (water-wet) as the water salinity decreased from 46.58 to 2.31 g/L. We concluded that the wettability of rock surface changed from oil neutral-wet to water-wet and induced the imbibition process, during which the hydrophilic pores absorbed the low-salinity water into the smaller pores.

2. RESULTS AND DISCUSSION

2.1. Initial Configuration of Fluid in the Pore Scale.
The initial configuration (before water flooding) of fluid in the pore-scale reservoir-on-a-chip is shown in Figure 1. The rock
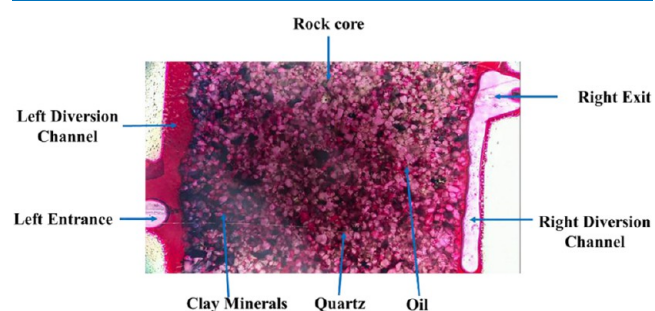

Figure 1. Full view of the reservoir-on-a-chip saturated with oil at the initial condition.

core in the chip consisted of three parts: oil (red), quartz (white), and clay mineral (black). The oil was injected into the model from the left entrance, and two diversion channels were set at both sides of the core to drive the oil and water evenly into the model.

2.2. Improved Sweep Efficiency by Low-Salinity Water Flooding.
Figure 2 presents five views of the remaining oil in the microchip. The results for remaining oil configuration after high- and low-salinity water flooding are
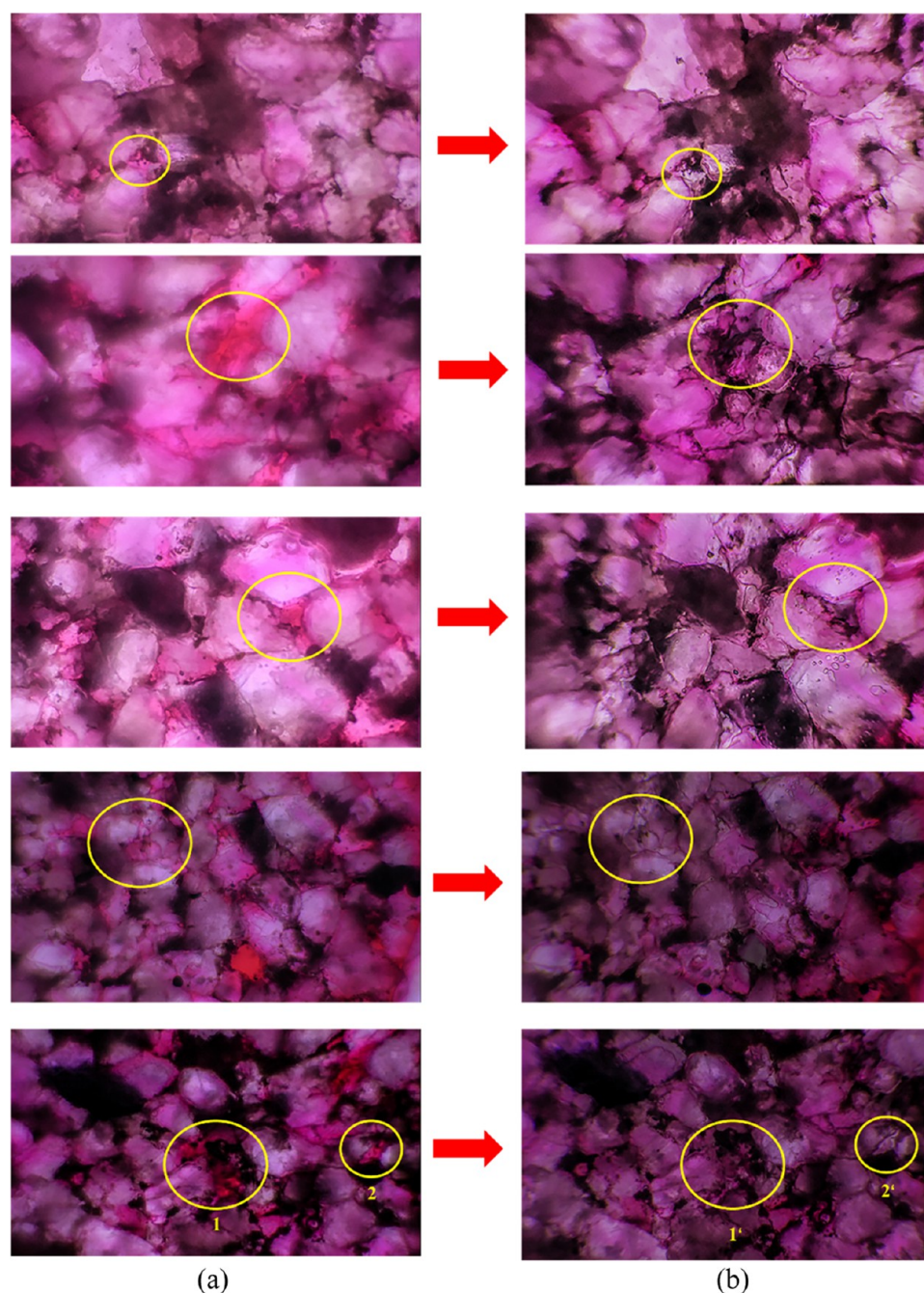
Figure 2. Oil configuration after high-salinity water flooding (a) and low-salinity water flooding (b).

presented in panels (a) and (b), respectively. As seen in Figure 2a, after flooding the chip with high-salinity water, the "mobile" oil in the main body of the chip has been recovered, but considerable initial oil was left in some smaller pores, such as circles 1 and 2. These areas are the un-swept area by the high-salinity water flooding, and the oils remained. After we injected low-salinity water into the chip, as seen in Figure 2b, the variation of remaining oil in the pores occurred. In circles 1′ and 2′, the remaining oil disappeared, which meant that low-salinity water invaded these areas and displaced the remaining oil.

Figure 3 presents another view of the difference of remaining oil between high- and low-salinity water flooding. Figure 3a presents the remaining oil after high-salinity water flooding, and Figure 3b presents the remaining oil after low-salinity

water flooding. The yellow circles marked the difference of remaining oil between high- and low-salinity water flooding. As shown in Figure 3a, after the chip flooded by high-salinity water, a significant amount of initial oil was flooded. However, it can be found that obvious oil remained in the un-swept area as marked by circle 1. As shown in Figure 3b, after flooded by low-salinity water, the remaining oil in the area marked by yellow circle 1′ has been flooded. The low-salinity water flooded into the un-swept area and improved the sweep efficiency. The mobilization of the remaining oil in the initially un-swept region indicated that the improved sweep efficiency might potentially be the major controlling factor of the enhanced oil recovery by low-salinity water flooding.

2.3. Mechanism of the Improved Sweep Efficiency. Figure 4a presents the result of contact angle for rock−crude
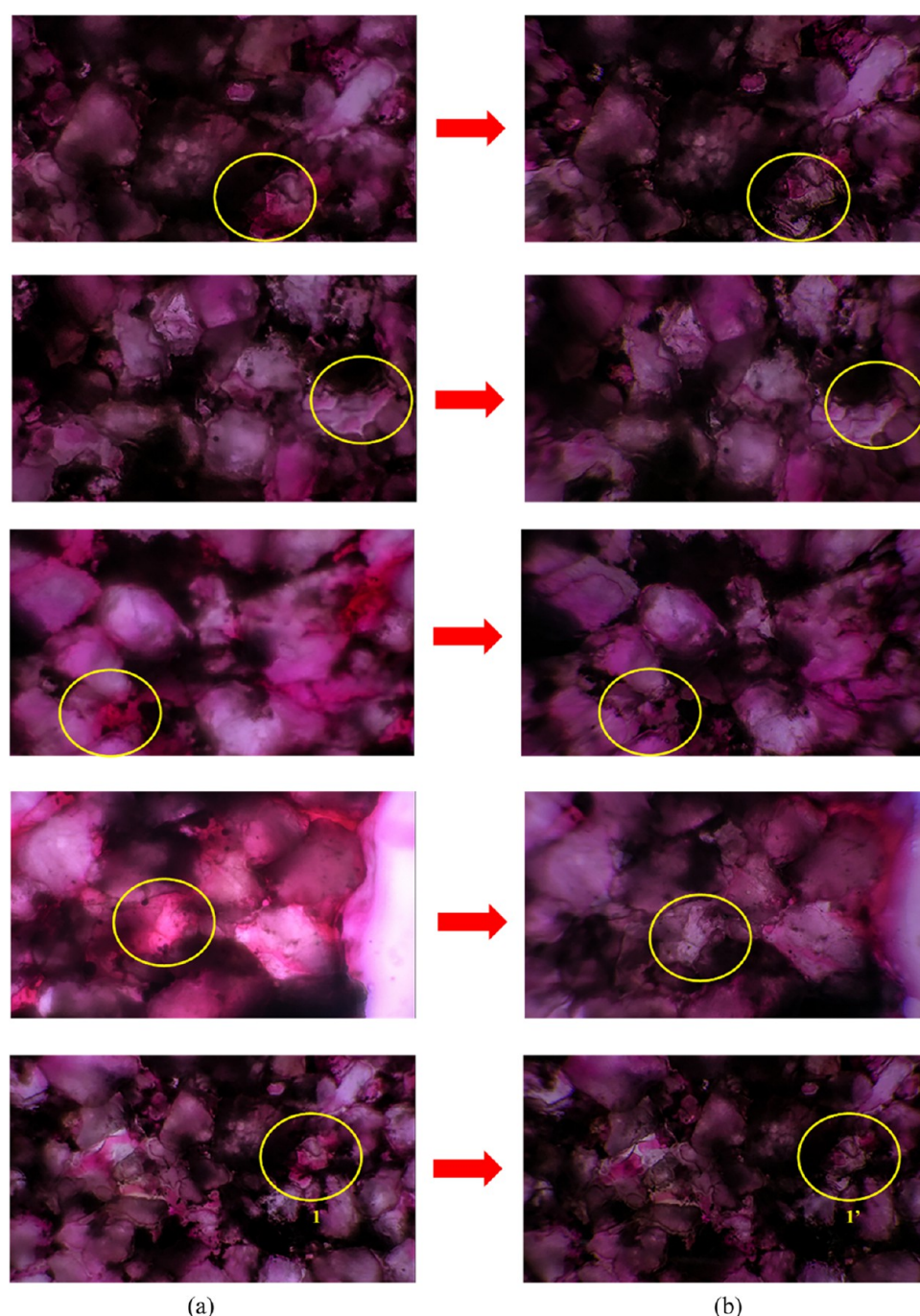
Figure 3. Difference of remaining oil between high-salinity water flooding (a) and low-salinity water flooding.

oil—high-salinity water (HSW), and Figure 4b presents the result of contact angle for rock—crude oil—low-salinity water (LSW). The contact angle in HSW was 91.05°, which meant that the wettability of the rock in HSW was neutral-wet. The contact angle in LSW was 64.41°, which meant that the wettability of the rock in LSW was water-wet. The contact angles decreased from 91.05 to 64.41° as the water salinity decreased from 46.58 to 2.31 g/L. It proved that low-salinity water could change the wettability in the chip from oil or neutral-wet to water-wet. Thus, we could conclude that the improvement of the sweep efficiency by low-salinity water flooding attributed to the wettability alteration from oil or neutral-wet to water-wet. During the water flooding process, wettability alteration from oil or neutral-wet to water-wet in a

real reservoir might result in the change of pore surface from hindering water displacing oil to promoting water displacing oil. Specifically, during the high-salinity water flooding, injected water must overcome the resistance to invade the pore to flood the oil as the pore surface was hydrophobic. On the contrary, during the low-salinity water flooding, the hydrophilic pores absorbed the low-salinity water into the smaller pores as the pore was hydrophilic. This is the reason why the low-salinity water can invade the un-swept pores beyond high-salinity water's utmost reach and displace the remaining oil after high-salinity water flooding.
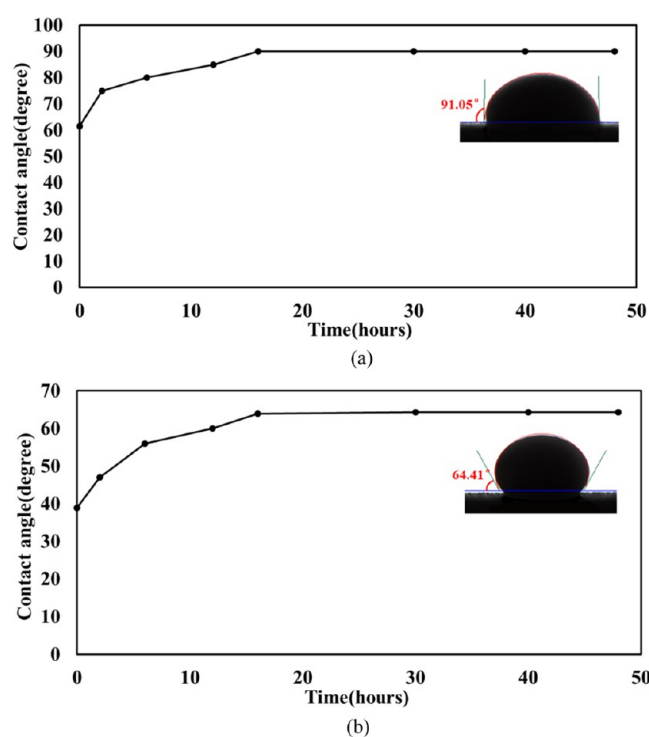
Figure 4. Contact angles for the rock-oil-high-salinity water (a) and rock-oil-low-salinity water (b)

3. EXPERIMENTS AND MATERIALS

3.1. Fluids. A crude oil taken from oil reservoirs diluted by kerosene with appropriate viscosity and density (viscosity, 1–1.5 cp; density, of 0.8 g/cm^3) was considered for contact angle tests and visual microfluidic experiment in this study. To eliminate any adversity related to rheology issue such as wax precipitations, the oil was heated up to 90 °C and then gradually settled at a reservoir temperature of 60 °C in the case the pores are blocked by the precipitates. Then, the resultant oil was filtered, centrifuged, and flowed through another filter installed at the inlet of the chip to make sure no precipitate entered into the micromodel. The diluted oil was dyed red by Sudan Red for observation, as seen in Figure 5. In terms of saturates, aromatics, resins, and asphaltenes (SARA) tests, Table 1 shows the SARA result of the crude oil.

Two different salinity synthetic brines were used in this study, including high-salinity water and low-salinity water. A synthetic brine with a salinity of 46.58 g/L was used as a high-salinity water in this study, and the low-salinity water with a
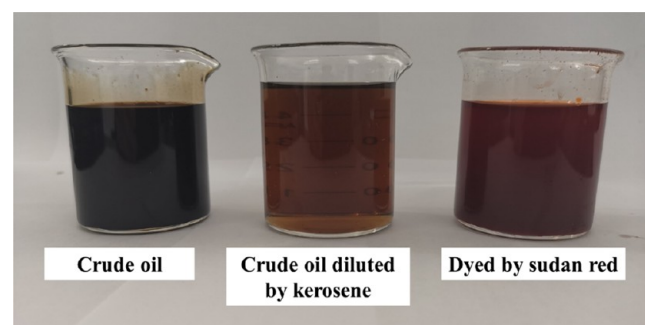

Figure 5. Pictures of crude oil (left), oil diluted by kerosene (middle), and diluted oil dyed by Sudan Red (right)

Table 1. Component of Crude Oil in This Experiment

component	alkane	aromatics	resins	asphaltene
mass fraction (%)	34.68	26.62	37.13	1.57

salinity of 2.31 g/L used in this study was diluted from this synthetic brine. These brines were made by mixing pure salts (Merck grade), including NaCl, CaCl$_2$, and MgCl$_2$, with distilled water. The amounts of salt in the brine are shown in Table 2.

Table 2. Components of Synthetic Brine in This Experiment

component	NaCl (g/L)	CaCl$_2$ (g/L)	MgCl$_2$ (g/L)	total salinity (g/L)
high-salinity water	37.64	7.56	1.38	46.58
low-salinity water	1.88	0.37	0.06	2.31

3.2. Rock. Traditional methods to fabricate a microfluidic model always select glass or calcite as the materials due to limitations in terms of technology, which means that a researcher must simplify the real complex component of the reservoir rock as SiO$_2$ or CaCO$_3$. Given that the traditional micromodel may not imitate the real component of the reservoir, in this study, we fabricated a real reservoir-on-a-chip using a core drilled from a reservoir in western China. The mineral compositions of the core are listed in Table 3 and

Table 3. Mineral Compositions of the Core

mineral	clays	quartz	glauberite	anorthose	augite	other minerals
mass fraction (%)	30.4	32.4	10.5	13.7	3.7	9.3

Figure 6. The reservoir-on-a-chip model consists of a rock core, import and export channels, and glass splints. The fabrication steps involved removing oil, core cutting, drying, polishing, and sealing.

3.3. Fabrication Steps. *3.3.1. Core Cutting and Removing Oil.* It is of utmost importance that the rock core must be cut very thin for observation. Meanwhile, it needs to retain the pore structure and feature of the rock core. In this step, the wire-cutting technique was used to cut the rock core, and the size of the rock core is 2.5 cm × 2.5 cm × 0.07 cm. To remove the original organic residue in the pores, we used a soxhlet extractor to clean the rock core for 3 days.

3.3.2. Drying. The core was dried in a constant-temperature cabinet for 3 days at 110 °C to remove the liquid in the pores.

3.3.3. Polishing. Both surfaces of the rock core must be polished as smooth as possible to make the surfaces of the core smooth and no knots. A 2000-mesh sandpaper was used in this step to polish the rock core, and high flow rate N$_2$ was used to blow the debris throughout the whole polishing process in case the debris blocked the pores.

3.3.4. Sealing. The rock core was sealed by two slides of glasses. First, we placed one glass as the bottom surface on a flat table and put the core on the center of the glass. Second, we uniform coated the surface uncovered by the core of the glass by appropriate glue, leaving the space for entrance and exit channels. Third, we covered the other glass on the bottom surface and clamped the two halves together until the glue dried. The final product is shown in Figure 7.
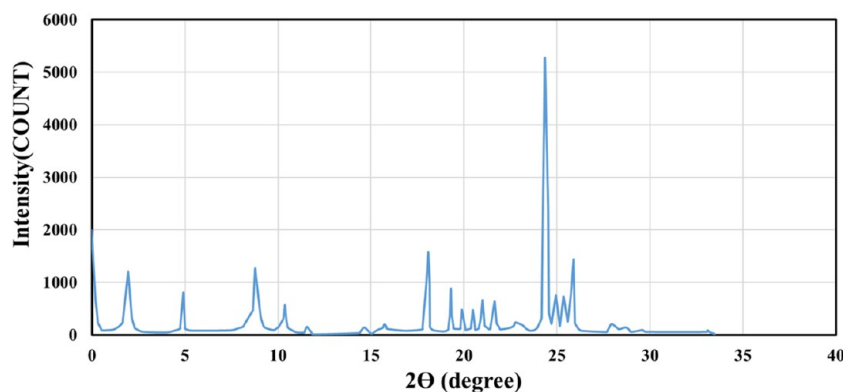
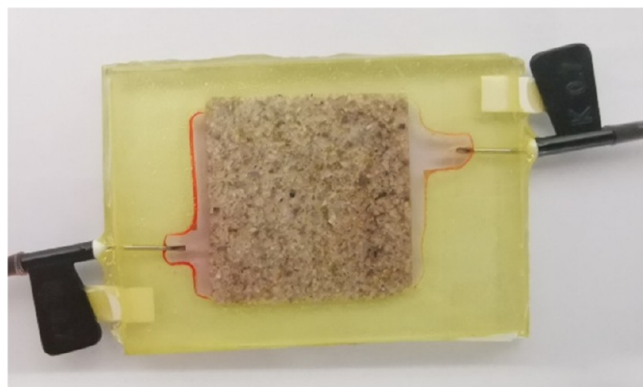**Figure 6.** X-ray diffraction (XRD) result of the rock composition analysis

Figure 7. Picture of the reservoir-on-a-chip

3.3.5. Performance Testing. The model was tested by sealing with injected N_2, and the gas pressure was maintained at 0.5 MPa for 15 h to prevent leakage. The permeability of the model was calculated as 2.5 mD by the Darcy formula, and the porosity is about 9.1%.

3.4. Experimental Setup. The microfluidic experimental setup was made of four systems, cleaning system, injecting system, monitoring system, and model system. The cleaning system included a piston pump and washing liquids with functions to inject washing liquids into the chip when an experiment finished. The injecting system included a piston pump and injecting liquids such as high-salinity water (HSW), low-salinity water (LSW), and crude oil with functions to inject fluids into the chip to imitate the water flooding process in the reservoir. The monitoring system included a high-resolution digital camera and a computer with functions to monitor and record the process of high- and low-salinity water flooding in real time. The model system included the reservoir-on-a-chip, a light source, and a liquid collector as shown in Figure 8.

As shown in Figure 9, the laboratory equipment of the contact angle experiment included a high-definition (HD) camera, an injection syringe, a sample cell, and a computer. The HD camera was used to capture the contact angle of rock–crude oil–brine system. The injection syringe was used to inject oil onto the surface of the rock plate. The sample cell was used to contain the salinity brine, and the computer was used to compute the contact angle and record the data.

3.5. Micromodel Test Procedure. *3.5.1. Injecting Oil.* The microfluidic experiment was carried out to imitate the water flooding performance by high- and low-salinity brine at room temperature and pressure. The chip was saturated with crude oil under the injected rate of 0.0002 mL/min for more
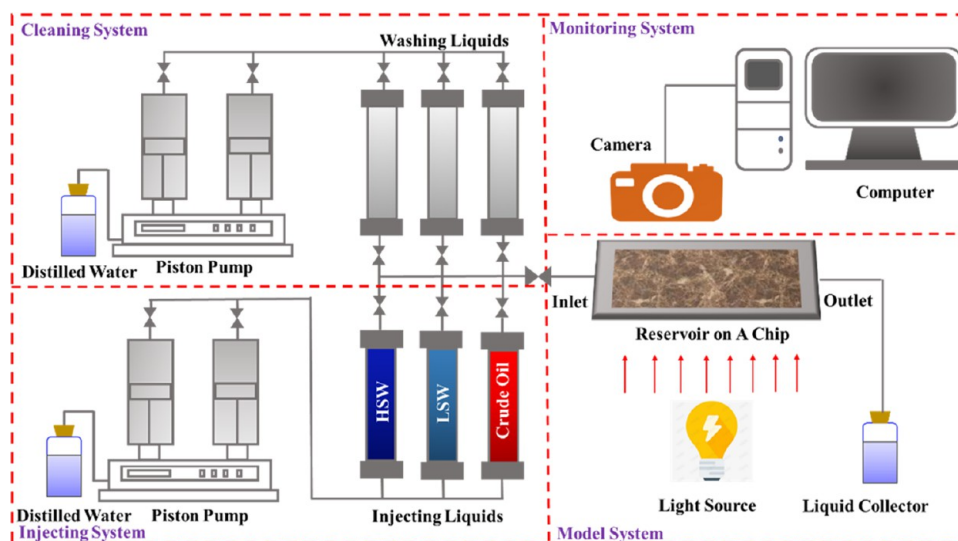

Figure 8. Schematic of the pore-scale reservoir-on-a-chip microfluidic experimental setup.
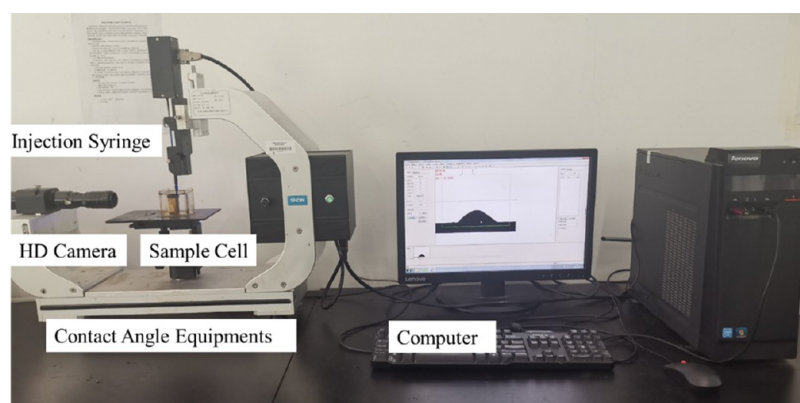
Figure 9. Laboratory equipment of the contact angle experiment

than 50 pore volume (PV) to make sure that all pores were filled with oil.

3.5.2. Aging. Before water flooding, the model was aged for 3 days at room temperature and pressure to imitate the oil-wet wettability in a reservoir.

3.5.3. HSW Flooding. High-salinity water was injected into the model under the injected rate of 0.0002 mL/min for more than 50 PV to displace all of the mobile oil and achieve the highest primary oil recovery. The injecting pressure was around 0.66 kPa according to the Darcy law.

3.5.4. LSW Flooding. Low-salinity water was injected under the same injecting rate to further displace the remaining oil, and the process of low-salinity water flooding was performed for 100 PV to maximize the effect of low-salinity water. The distribution and configuration characteristics of the remaining oil during the water flooding process were recorded by the camera and the computer in real time.

3.6. Contact Angle Tests Procedure. The aim of the contact angle tests was to verify the wettability alteration by low-salinity water flooding. A rock plate cut from the same core used to make the microchip was first polished to remove the surface roughness to perform the tests. The captive drop method was used to attach an oil droplet to the plate and measure contact angle. The contact angle was first measured with high-salinity water. The rock plate was placed in the water cell filled with high-salinity water for 1 day to age. Then, a crude oil droplet was released using a U-shaped syringe needle to the subsurface of the rock plate. The oil droplet then started to age, and the contact angle was continuously monitored until reaching equilibrium. The aging process usually lasted for 2 days. The same procedure was repeated for the measurement of low-salinity water contact angle.

4. CONCLUSIONS

A pore-scale reservoir-on-a-chip water flooding experiment and contact angle experiments were conducted to investigate the pore-scale mechanism of the improved sweep efficiency by low-salinity water flooding. The main conclusions and novel insights in this study are:

(1) High-salinity water flooding cannot thoroughly flood the whole pore space in a reservoir during the water flooding process, and a significant amount of oil remained in the un-swept region.

(2) Low-salinity water flooding can invade the pores that cannot be reached by high-salinity water and displace the remaining oil after high-salinity water flooding, and

the controlling factor of the enhanced oil recovery by low-salinity water flooding may be the improvement of the sweep efficiency.

(3) Contact angle experiments show that the wettability of the crude oil–brine–rock can be changed from oil or neutral-wet to water-wet by injecting low-salinity water flooding. The pore surface turns from hydrophobic to hydrophilic.

(4) Wettability alteration from oil-wet to water-wet is the mechanism of the improved sweep efficiency by low-salinity water flooding. During the process of high-salinity water flooding, the hydrophobic pore surface hinders the water to invade the pore. However, low-salinity water flooding induces the imbibition process, during which the hydrophilic pore surface absorbs the low-salinity water into the pores un-swept by high-salinity water.

■ AUTHOR INFORMATION

Corresponding Authors

Yuetian Liu − *State Key Laboratory of Petroleum Resources and Prospecting, China University of Petroleum, Beijing 102249, China;* orcid.org/0000-0002-9431-1031; Email: lyt51@163.com

Liang Xue − *State Key Laboratory of Petroleum Resources and Prospecting, China University of Petroleum, Beijing 102249, China;* Email: xueliang@cup.edu.cn

Authors

Songqi Li − *State Key Laboratory of Petroleum Resources and Prospecting, China University of Petroleum, Beijing 102249, China;* orcid.org/0000-0002-5652-5020

Li Yang − *CNOOC Research Institute Co., Ltd., Beijing 100028, China*

Zhiwang Yuan − *CNOOC Research Institute Co., Ltd., Beijing 100028, China*

Complete contact information is available at:
https://pubs.acs.org/10.1021/acsomega.1c02511

■ **REFERENCES**

(1) Seyyedi, M.; Tagliaferri, S.; Abatzis, J.; Nielsen, S. M. An integrated experimental approach to quantify the oil recovery potential of seawater and low-salinity seawater injection in North Sea chalk oil reservoirs. *Fuel* **2018**, 267−278.

(2) Li, S.; Liu, Y.; Xue, L.; Yang, L.; Yuan, Z.; Jian, C. An investigation on water flooding performance and pattern of porous carbonate reservoirs with bottom water. *J. Pet. Sci. Eng.* **2021**, No. 108353.

(3) Zaeri, M. R.; Hashemi, R.; Shahverdi, H.; Sadeghi, M. Enhanced oil recovery from carbonate reservoirs by spontaneous imbibition of low salinity water. *Pet. Sci.* **2018**, 564−576.

(4) Olayiwola, S. O.; Dejam, M. A comprehensive review on interaction of nanoparticles with low salinity water and surfactant for enhanced oil recovery in sandstone and carbonate reservoirs. *Fuel* **2019**, 1045−1507.

(5) Zhang, W.; Ning, Z.; Zhang, B.; Wang, Q.; Cheng, Z.; Huang, L.; Qi, R.; Shang, X. Experimental investigation of driving brine water for enhanced oil recovery in tight sandstones by DC voltage. *J. Pet. Sci. Eng.* **2019**, 485−494.

(6) Zhang, W.; Ning, Z.; Cheng, Z.; Wang, Q.; Wu, X.; Huang, L. Experimental Investigation of the Role of DC Voltage in the Wettability Alteration in Tight Sandstones. *Langmuir* **2020**, *36*, 11985−11995.

(7) Lee, J. H.; Lee, K. S. Geochemical evaluation of low salinity hot water injection to enhance heavy oil recovery from carbonate reservoirs. *Pet. Sci.* **2019**, 366−381.

(8) Wang, H.; Tian, L.; Gu, D.; Li, M.; Chai, X.; Yang, Y. Method for Calculating Non-Darcy Flow Permeability in Tight Oil Reservoir. *Transp. Porous Media* **2020**, 357−372.

(9) Jafari, A.; Hasani, M.; Hosseini, M.; Gharibshahi, R. Application of CFD technique to simulate enhanced oil recovery processes: current status and future opportunities. *Pet. Sci.* **2020**, 434−456.

(10) Ayirala, S.; Alghamdi, A.; Gmira, A.; Cha, D. K.; Alsaud, M. A.; Yousef, A. Linking pore scale mechanisms with macroscopic to core scale effects in controlled ionic composition low salinity waterflooding processes. *Fuel* **2020**, No. 116798.

(11) Qin, Z.; Arshadi, M.; Piri, M. Micro-scale experimental investigations of multiphase flow in oil-wet carbonates. I. In situ wettability and low-salinity waterflooding. *Fuel* **2019**, No. 116014.

(12) Bartels, W.-B.; Mahani, H.; Berg, S.; Hassanizadeh, S. M. Literature review of low salinity waterflooding from a length and time scale perspective. *Fuel* **2019**, 338−353.

(13) Bartels, W.-B.-B.; Mahani, H.; Berg, S.; Menezes, R.; van der Hoeven, J. A.; Fadili, A. Oil Configuration Under High-Salinity and Low-Salinity Conditions at Pore Scale: A Parametric Investigation by Use of a Single-Channel Micromodel. *SPE J.* **2017**, *22*, 1362−1373.

(14) Le-Anh, D.; Rao, A.; Ayirala, S. C.; Alotaibi, M. B.; Duits, M. H. G.; Gardeniers, H.; Yousef, A. A.; Mugele, F. Optical measurements of oil release from calcite packed beds in microfluidic channels. *Microfluid. Nanofluid.* **2020**, No. 47.

(15) Liu, F.; Wang, M. Review of low salinity waterflooding mechanisms: Wettability alteration and its impact on oil recovery. *Fuel* **2020**, No. 117112.

(16) Su, W.; Liu, Y.; Pi, J.; Chai, R.; Li, C.; Wang, Y. Effect of water salinity and rock components on wettability alteration during low-salinity water flooding in carbonate rocks. *Arabian J. Geosci.* **2018**, *11*, No. 260.

(17) Mohammadi, M.; Mahani, H. Direct insights into the pore-scale mechanism of low-salinity waterflooding in carbonates using a novel calcite microfluidic chip. *Fuel* **2020**, No. 116374.

(18) Du, Y.; Xu, K.; Mejia, L.; Zhu, P.; Balhoff, M. T. Microfluidic Investigation of Low-Salinity Effects During Oil Recovery: A No-Clay and Time-Dependent Mechanism. *SPE J.* **2019**, *24*, 2841.

(19) Mahzari, P.; Sohrabi, M.; Cooke, A. J.; Carnegie, A. Direct pore-scale visualization of interactions between different crude oils and low salinity brine. *J. Pet. Sci. Eng.* **2018**, 73−84.

(20) Aldousary, S.; Kovscek, A. R. The diffusion of water through oil contributes to spontaneous emulsification during low salinity waterflooding. *J. Pet. Sci. Eng.* **2019**, 606−614.

(21) Barnaji, M. J.; Pourafshary, P.; Rasaie, M. R. Visual investigation of the effects of clay minerals on enhancement of oil recovery by low salinity water flooding. *Fuel* **2016**, 826−835.

(22) Alfi, M.; Nasrabadi, H.; Banerjee, D. Experimental investigation of confinement effect on phase behavior of hexane, heptane and octane using lab-on-a-chip technology. *Fluid Phase Equilib.* **2016**, 25−33.

(23) Mehraban, M. F.; Farzaneh, S. A.; Sohrabi, M.; Sisson, A. Novel Insights into the Pore-Scale Mechanism of Low Salinity Water Injection and the Improvements on Oil Recovery. *Energy Fuels* **2020**, *34*, 12050−12064.

(24) Mehraban, M. F.; Farzaneh, S. A.; Sohrabi, M. Debunking the Impact of Salinity on Crude Oil/Water Interfacial Tension. *Energy Fuels* **2021**, *35*, 3766−3779.

(25) Sanyal, S.; Bhui, U. K.; Kumar, S. S.; Balaga, D. Designing Injection Water for Enhancing Oil Recovery from Kaolinite Laden Hydrocarbon Reservoirs: A Spectroscopic Approach for Understanding Molecular Level Interaction during Saline Water Flooding. *Energy Fuels* **2017**, *31*, 11627−11639.

(26) Sanyal, S.; Bhui, U. K.; Balaga, D.; Kumar, S. S. Interaction study of montmorillonite-crude oil-brine: Molecular-level implications on enhanced oil recovery during low saline water flooding from hydrocarbon reservoirs. *Fuel* **2019**, No. 115725.

(27) Sanyal, S.; Singh, K. A.; Parekh, H.; Chokshi, V.; Bhui, U. K. Interaction study of clay-bearing amphibolite−crude oil−saline water: Molecular level implications for enhanced oil recovery during low saline water flooding. *J. Earth. Syst. Sci.* **2018**, *127*, No. 112.

(28) Sanyal, S.; Anjirwala, H.; Bhatia, M.; Lalnuntluanga; Shah, D.; Vyas, D.; Bhui, U. K. Interaction of Clay−Crude Oil−Injection Brine: An Experimental Approach for Understanding the Effectiveness of Low Saline Water (LSW) During Enhanced Oil Recovery (EOR). In *Macromolecular Characterization of Hydrocarbons for Sustainable Future. Green Energy and Technology*; Bhui, U. K., Ed.; Springer: Singapore, 2021.

(29) Song, W.; Kovscek, A. R. Functionalization of micromodels with kaolinite for investigation of low salinity oil-recovery processes. *Lab Chip* **2015**, 3314−3325.